small methods
www.small-methods.com

Check for updates

Wafer-Scale Fabrication of Nanopore Devices for Single-Molecule DNA Biosensing using MoS_2

*Mukeshchand Thakur, Michal Macha, Andrey Chernev, Michael Graf, Martina Lihter, Jochem Deen, Mukesh Tripathi, Andras Kis, and Aleksandra Radenovic**

Atomically thin (2D) nanoporous membranes are an excellent platform for a broad scope of academic research. Their thickness and intrinsic ion selectivity (demonstrated for example in molybdenum disulfide-MoS_2) make them particularly attractive for single-molecule biosensing experiments and osmotic energy harvesting membranes. Currently, one of the major challenges associated with the research progress and industrial development of 2D nanopore membrane devices is small-scale thin-film growth and small-area transfer methods. To address these issues, a large-area protocol including a wafer-scale monolayer MoS_2 synthesis, Si/SiN_x substrate fabrication and wafer-scale material transfer are demonstrated. First, the 7.62 cm wafer-scale MOCVD growth yielding homogenous monolayer MoS_2 films are introduced. Second, a large number of devices are fabricated in one batch by employing the wafer-scale thin-film transfer method with high transfer efficiency (>70% device yield). The growth, the transfer quality and cleanliness are investigated using transmission electron microscopy, atomic force microscopy and Raman spectroscopy. Finally, the applicability and robustness of the large-area protocol is demonstrated by performing a set of double-stranded DNA translocation experiments through as-fabricated MoS_2 nanopore devices. It is believed that the shown approach will pave the way toward wafer-scale, high-throughput use of 2D nanopores in various applications.

1. Introduction

Nanopore-based sensing is attractive in the field of single-molecule detection as it offers low-cost, label-free, and high-throughput analysis. In general, a nanopore device is a small nanometric aperture separating two compartments filled with ionic solutions. When a bias voltage is applied, an electrically charged molecule (e.g., DNA) electrophoretically threads through the nanopore. This process generates a transient resistive pulse in the ion current, which can be used to study the translocation of a single molecule. Based on their composition, nanopores are categorized as biological, silicon- or polymer-based solid-state pores or DNA-origami pores.[1–4] One of the promising applications of nanopore devices is DNA sequencing, often regarded as the fourth-generation sequencing technology. So far, only biological nanopores have been used for commercial sequencing applications.[5,6] Since the functional unit of these biological nanopores are protein channels, their stability in the lipid-bilayer is limited by the ionic strength of the electrolyte, the voltage that can be applied, chemical, mechanical, and thermal stability. In contrast, solid-state nanopores are more mechanically and chemically robust, providing flexibility in working with higher voltages, ionic concentrations and temperatures. Their size can be precisely tuned for a desired application and on top of that, they can be fabricated in sizable arrays, potentially improving the sensing efficiency. To improve the spatial and temporal resolution of detection, for biopolymers such as DNA, the thickness and the pore diameter of the sensing membrane needs to be comparable with the lateral diameter of the biopolymer. In this regard, 2D materials such as graphene,[7,8] hexagonal boron nitride,[9] and transition metal dichalcogenides (TMDs) materials such as tungsten disulfide (WS_2)[10] and molybdenum disulfide (MoS_2)[11–16] were explored as 2D solid-state nanopores. MoS_2, in particular, is interesting since it is composed of three-atoms (≈0.65 Å).[17] In addition to the thickness, the presence of hydrophilic molybdenum atoms at the pore facilitates the base differentiation. Furthermore, DNA tends to interact less with the membrane surface when compared to graphene.[18] And lastly, the signal-to-noise ratio in MoS_2 is higher than in other 2D materials.[11,18] All these reasons make MoS_2 an attractive and widely studied 2D material for DNA biosensing application. Experimentally, using a gradient of room temperature ionic liquids and KCl solution,

M. Thakur, M. Macha, Dr. A. Chernev, Dr. M. Graf, Dr. M. Lihter, Dr. J. Deen, Prof. A. Radenovic
Institute of Bioengineering
Laboratory of Nanoscale Biology
School of Engineering
EPFL
Lausanne 1015, Switzerland
E-mail: aleksandra.radenovic@epfl.ch

Dr. M. Tripathi, Prof. A. Kis
Laboratory of Nanoscale Electronics and Structure
Institute of Electrical Engineering and Institute of Materials Science and Engineering
School of Engineering
EPFL
Lausanne 1015, Switzerland

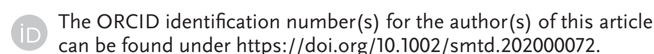
The ORCID identification number(s) for the author(s) of this article can be found under https://doi.org/10.1002/smtd.202000072.

DOI: 10.1002/smtd.202000072

 © 2020 WILEY-VCH Verlag GmbH & Co. KGaA, Weinheim

monolayer MoS_2 nanopore devices have achieved single-nucleotide differentiation.[12] Furthermore, monolayer MoS_2 nanopore devices are becoming promising tools for emerging scientific applications in defect-engineering research[19–23] and highly efficient blue energy harvesting.[24–26]

One of the most crucial bottlenecks of monolayer device fabrication is the thin film synthesis and its processing scale. Most reported applications rely on a relatively small monolayer substrate size which enforces a single-chip transfer and fabrication of a single device a time.[10–12,14,27] This approach is highly time consuming and cost ineffective, especially if the application requires a significant number of devices. Likewise, even if a uniform thin film growth is performed on a large substrate area, without an easy and repeatable large-scale transfer method the same problem remains. Hence, a large-scale approach toward the production of robust, low-cost and scalable nanopore devices is paramount to ensure high research yield and scientific progress in this field. Currently, the major challenges associated with 2D MoS_2 nanopore devices are their high-quality and defect-free synthesis, sensing noise associated with device architecture, and variability in the fabricated devices in terms of pore size, pore geometry and thickness. These problems, usually occurring with 2D materials requiring require a clean large-scale microfabrication process.

In this work, we address these challenges by growing large-area continuous MoS_2 films on a 7.62 cm sapphire substrate with subsequent wafer-scale transfer using polydimethylsiloxane (PDMS). The growth process is based on metalorganic chemical vapor deposition (MOCVD). By using the c-plane sapphire substrates, high-purity gaseous phase precursors and an alkaline salt as a growth catalyst, we obtain the reproducible and highly efficient synthesis of continuous mono- to few-layer MoS_2 films. For the transfer of MoS_2 films, we use PDMS as a supporting polymer along with water, avoiding any hazardous etchants (e.g., KOH) or additional etching steps during transfer. The transfer process is less labor intensive and does not need any additional expensive instruments usually used in existing deterministic transfer methods.[14,28] Furthermore, the MoS_2 growth substrate is recyclable thereby reducing the substrate costs. In combination with PDMS transfer, we demonstrate cost-effective and time-efficient method for large-scale nanopore-device fabrication (a total of 128 devices per batch) with successful transfer yield (>70%). The 2D material quality and cleanliness of the wafer-scale transferred MoS_2 was evaluated with high-resolution transmission electron microscopy (HRTEM) and aberration-corrected scanning transmission electron microscopy (STEM) imaging. We have found that transfer quality is comparable to the well-established, small-scale PMMA-based techniques[14,19] and can be adapted to other polymer materials.

2. Results and Discussion

2.1. Wafer-Scale MoS_2 Growth and Transfer

For the 2D material synthesis, we have used a modified and upscaled methodology based on a combination of two different approaches. The first one uses the metalorganic precursor (molybdenum hexacarbonyl $Mo(CO)_6$) and diethyl sulfide (DES) as molybdenum and sulfur sources,[29] respectively. The second one relies on the addition of spin-coated liquid-phase growth promoters, sodium molybdate (Na_2MoO_4) and alkaline salt, prior to the growth phase.[30,31] Using a spin-coated Na_2MoO_4 solution both to ensure uniform seeding and as an additional molybdenum source during growth step yields highly homogenous, large 2D crystals of MoS_2, leading to continuous monolayer formation under proper process parameters. The use of alkaline salts as a crystal growth catalyst is a common practice in the MoS_2 synthesis protocols,[32–34] which lowers the density of nucleation sites and the melting point of the solid-state precursors. This results in an increase of the final crystal size by orders of magnitude. In particular, NaCl is an advantageous addition to the growth. Under elevated temperature, it can form intermediate ternary species with molybdenum acting as planar, cyclic seeding promoters both suppressing the nucleation and increasing lateral crystal growth rate on the target substrate.[34]

Taking advantage of both of these approaches, we have used a spin-coated mixture of both Na_2MoO_4 and NaCl as a continuous growth promoter. Prior to the growth, annealed and hydrophilized (see Experimental Section) c-plane sapphire wafers (7.62 cm) were coated with promoter solution to achieve a uniform layer. Typical growth step is performed in a homemade MOCVD, hot-wall, vertical furnace for 30 min at 850 °C under the flow of 210 sccm of Ar, 1 sccm of O_2, 4 sccm of H_2 (Figure S1, Supporting Information). In contrast to previous publications,[30,31,34] we are adding several new elements and improvements to our process. First, we use separate bubblers for $Mo(CO)_6$ and DES, which increases the control in delivering the gases into the chamber, and 12 sccm of Ar is flowing through a bubbler filled with, $Mo(CO)_6$, and 3 sccm of Ar through separate DES bubbler. Second, the sapphire substrate is placed vertically to achieve uniform exposure to the gases and homogeneous reaction conditions. The combination of the metal-organic gaseous precursor, the sulfur-rich atmosphere, and the Na_2MoO_4 solution uniformly coated on the substrate, ensures a uniform seeding of MoS_2 across the whole substrate and a steady supply of Mo mass, promoting large-scale, continuous film formation with a high degree of control. The addition of NaCl to the spin-coating solution ensures a high reaction rate and a low nucleation density, which as a result increases the overall grain size, visible through merged, extruded grain boundaries, and single crystals on the edges of the substrate. A moderate amount of hydrogen is necessary to help decomposing the DES and $Mo(CO)_6$ ligands and to prohibit carbon containing reaction products from depositing on the substrate. Lastly, we are introducing small amounts of oxygen to the process, which ensures smooth grain mergers, decreases the probability of a secondary layer formation, and further limits the nucleation density due to local etching of unsteady nuclei.[30] The thickness of the continuous MoS_2 film can be controlled both with the concentration ratio of Na_2MoO_4/NaCl and the flow of O_2 (Figure S2, Supporting Information), and can range from single flakes to continuous multilayer. As a result, this method allows to repeatedly and efficiently produce large area mono- and multilayer MoS_2 alike.

The substrate fabrication process is detailed in the Experimental Section and Figure S3 (Supporting Information).

© 2020 WILEY-VCH Verlag GmbH & Co. KGaA, Weinheim

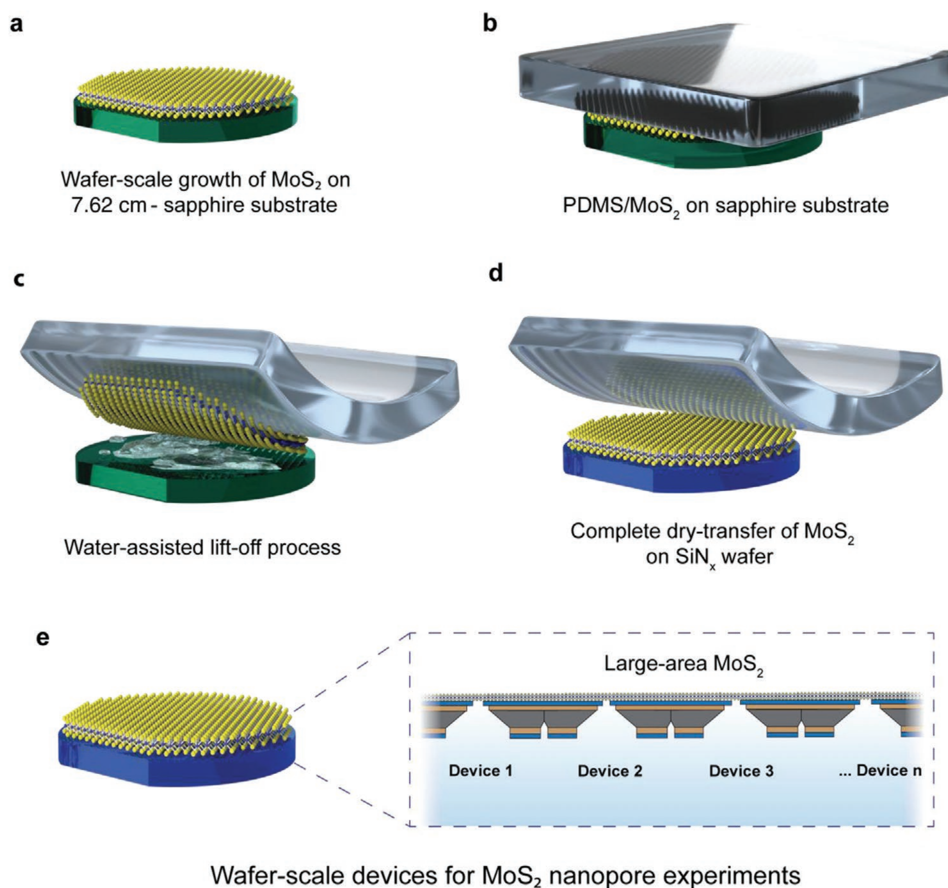

Figure 1. Illustration showing the wafer-scale PDMS-transfer of MoS_2 from a 7.62 cm sapphire wafer to a silicon substrate containing an array of SiN_x membranes with apertures. The objects are not to scale. a) Large-area MoS_2 on the growth substrate. b) The PDMS stamp is aligned to the MoS_2/sapphire substrate. c) Lift-off process where the water penetrates the interface between sapphire and MoS_2, while using a step-motor the PDMS/MoS_2 is lifted off. d) Dry transfer of large-area MoS_2 on the SiN_x wafer achieved by stamping using PDMS. e) Large-area MoS_2 transferred to the target substrate now containing devices that can be used for the nanopore experiments.

Each fabricated silicon wafer results in >120 devices where each device has one single aperture in a thin SiN_x membrane. In order to assess the variability of these apertures, we have characterized the apertures from different parts of the wafer using TEM. The size of the aperture is ≈75 nm within 5% error (Figure S4, Supporting Information).

The next step is the large-scale transfer of MoS_2 to the Si/SiN_x wafer. **Figure 1** depicts the steps involved in this process. The lift-off step is based on a surface-energy assisted transfer of MoS_2 using water[14,35–38] with a step-controlled translating stage (see Experimental Section). The material transfer is performed by aligning the PDMS onto the as-grown MoS_2 growth substrate (Figure 1a,b). The next step comprises of manually placing of MoS_2/PDMS layer in a container with water and lifting-off as water penetrates at the interface between the MoS_2 and the sapphire substrate (Figure 1c). Due to the surface interaction between MoS_2/PDMS (hydrophobic) and sapphire (hydrophilic), the water preferentially penetrates between MoS_2 and the sapphire substrate enabling the surface-energy based lift-off of MoS_2.[14,36] In the absence of water, the MoS_2 does not attach to the PDMS completely. Subsequently, MoS_2 is manually stamped on the SiN_x surface completing the large-area transfer.[14,39] It must be noted that during the transfer steps, we used the lift-off and stamping speed in the range of 5–10 µm s^{-1} (Figure 1c,d). One of the advantages of wafer-scale transfer is that unlike deterministic transfer methods,[14,40] this approach is simple and does not require any precise optical alignment setup. While wet-etching based wafer-scale transfer using polymers such as poly(methyl methacrylate) (PMMA) was recently demonstrated for MoS_2,[41] it requires surface modification of the growth substrate and an additional substrate etching step which may deteriorate the thin 2D material due to the harsh etchants used (e.g., KOH). In addition, PMMA coating was shown to have a time-dependant corrosive effect on the coated 2D materials, which can lead to poor device performance.[42] Furthermore, due to the thickness of thin PMMA films (several hundreds of nanometers), the wet transfer processes are prone to unwanted crumbling of the material, decreasing the transfer efficiency.[43] The PDMS, being significantly thicker (1–2 mm), but still flexible and optically transparent, provides a better mechanical stability, increasing transfer efficiency.[14,28,44] Previous reports have demonstrated small-scale deterministic transfer of TMDs using a micromanipulator stage using both PDMS and PMMA.[14,27,28,45]

 © 2020 WILEY-VCH Verlag GmbH & Co. KGaA, Weinheim

2.2. Characterization of MoS_2 Films

Optical images of as-grown MoS_2 (Figure S5, Supporting Information) show a uniform layer of film with rare secondary nucleation spots. Using sapphire as a substrate ensures epitaxial connection on the MoS_2/sapphire interface due to crystal lattice match.[33] However, Na-based compounds assisting the MoS_2 growth were reported to diminish such an epitaxial interface due to Na intercalation under the grown film large-area epitaxial monolayer.[46] Indeed, optical images (Figure S5, Supporting Information) reveal rare spots of extruded grain boundaries, which suggests imperfect grain stitching. Nonetheless, for our application, we have not observed any odd grain boundaries nor low-quality suspended areas on fabricated membrane devices. In our case, the sapphire substrate was (depending on the batch) ≈90–100% covered with continuous mono- to few-layer films (**Figure 2**a) which were transferred to the SiN_x substrates (Figure 2b).

To further inspect the large-scale growth quality and uniformity, Raman spectroscopy was performed across the whole wafer pre- and post-transfer (Figure 2c,d). The relative distance between in-plane E^1_{2g} and out-of-plane acoustic phonon modes is an indicator of MoS_2 thickness.[27,41] In our case, the average separation between E^1_{2g} and A_{1g} peaks remains in the range of 19.5–20.5 cm^{-1}, suggesting a uniform monolayer character of the film across the entire substrate. The absence of a peak separation difference between the spectra before and after the transfer is an indication of the non-destructive character of the transfer method. We observe, however, a small increase in E^1_{2g}/A_{1g} intensity ratios after the transfer, which can be due to changes in exciton-phonon interaction with the supporting substrate[47] or doping by charge transfer.[48] Additionally, to analyze the uniformity or the quality of the MoS_2 films, photoluminescence (PL) measurements were performed at the similar regions (labeled in Figure 2a,b) before and after the transfer (Figure S6, Supporting Information). The PL peaks did not show any significant shift (<5 nm) before and after transfer process indicating that the crystal quality of the layers did not deteriorate after the transfer.[41,49] These results are in corroboration with the Raman measurements. This may be attributed to the mild conditions used in the water-assisted transfer process that avoids the use of any harsh etchants, preserving the

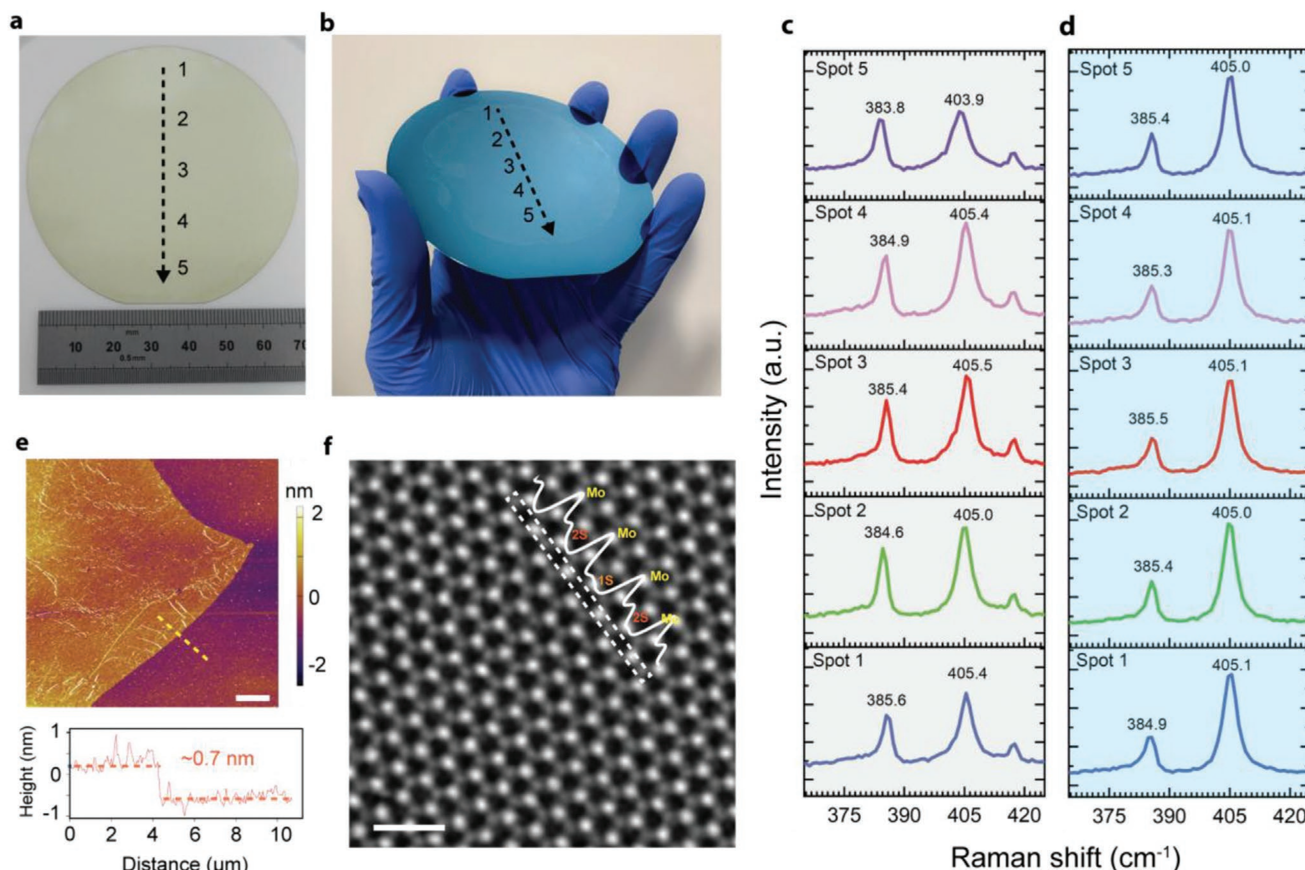

Figure 2. Characterization of large-area MoS_2 films. a) Continuous MoS_2 film grown on a sapphire substrate. b) Large-area wafer-scale transfer of MoS_2 over a silicon wafer with 128 SiN_x membranes containing apertures. The blue contrast of the MoS_2 transferred from the growth substrate is visible on the SiN_x surface. c,d) Raman spectroscopy from the same region of the wafer before (gray panel) and after the transfer (blue panel) of the MoS_2 films (unmarked peak around 420 cm^{-1} on a before-transfer spectra is a signature peak of the Al_2O_3 substrate used for the MoS_2 synthesis). e) AFM analysis showing monolayer MoS_2 post-transfer with ≈0.7 nm height profile. Scale bar is 6 µm. f) Double Gaussian filtered STEM image after transfer showing a clean MoS_2 lattice structure. Due to its Z-contrast dependency, the lattice structure can be directly inferred from the molybdenum atom (brighter) and the sulfur atom (darker) contrasts. A few intrinsic sulfur-vacancies can be directly observed in the image (inset: Intensity peak profile along the line for selected atoms showing one sulfur vacancy). Scale bar is 1 nm.

© 2020 WILEY-VCH Verlag GmbH & Co. KGaA, Weinheim

quality of the MoS_2 films.[41] The AFM surface characterization reveals ≈0.7 nm thick layers after the transfer, corresponding to the thickness of monolayer MoS_2(Figure 2e).[17] Aberration-corrected STEM is a well-established method to characterize the structural uniformity at atomic scale in low-dimensional materials including MoS_2, h-BN and graphene.[50–52] The STEM image (Figure 2f) shows the crystal lattice structure of a monolayer MoS_2 film. Due to the annular dark field contrast dependency, the intensity of the atomic columns can be directly interpreted since it is directly proportional to $Z^{1.6\text{-}2.0}$ (where Z is the atomic number).[50] Thus, Mo-atomic sites appear brighter in intensity than the sites where two sulfur atoms are on top of each other. The intensity profile along the line shows the peak positions of the Mo-atoms and S-atoms, respectively. To avoid electron-beam induced knock-on damage, a low acceleration voltage (80 kV) was used during the imaging.[53] A few intrinsic S-vacancies can be observed in the image,[54] further confirming the high-quality growth of our MoS_2 films (also shown in the line profile in Figure 2f). Furthermore, to assess the cleanliness of the suspended transferred MoS_2 regions, larger areas were analyzed where large-area clean regions with MoS_2 films can be observed with some polymer contamination (see Figure S7, Supporting Information). Due to advancements of aberration-correction, a smaller sized electron-beam probe (full width half maximum, FWHM, ≈1 Å) in STEM can be intentionally placed on the clean MoS_2 regions to create nanopores with tunable sizes in a controlled way by sputtering the atoms, for instance Panel 4 in Figure S7 (Supporting Information) shows a nanopore (≈2 nm^2) formed by the electron-probe.

2.3. Wafer-Scale Transfer Efficiency

The wafer-scale MoS_2 transfer efficiency of >70% device yield was calculated as the percentage of devices that have an aperture fully covered with MoS_2 (**Figure 3**a). Variation from batch to batch is shown in a Table S1 (Supporting Information). Two optical images of devices without MoS_2 (Figure 3b) and with MoS_2 (Figure 3c) show large-area MoS_2 transferred over the SiN_x membrane. Representative devices analyzed by TEM imaging are shown in Figure 3d. For devices, where the transfer process was unsuccessful as shown in Figure S8 (Supplementary Information), it is possible to use a chip-scale deterministic transfer method[14] to increase the device yield. The transfer efficiency can be enhanced by a slow lift-off process and a high monolayer coverage of the MoS_2 on the growth substrate.

One of the biggest challenges is to obtain residue-free transfer, since it affects the electronic properties of 2D materials. This surface contamination originate from the transfer methods using sacrificial polymer coatings (e.g., PDMS or PMMA) as shown in Figure S9 (Supplementary Information).[14,55] During the transfer, polymer layer is in direct contact with the MoS_2 which inevitably leads to residual surface contamination on the monolayer film.[44] Additional contamination source are airborne hydrocarbon contaminants adsorbing on the MoS_2 layers when exposed to air.[56,57] The device cleanliness can be improved by transfer strategies, which avoid the use of polymers.[58] However, such methods are not compatible with the large-area transfer because the thin 2D material films without polymer support can cause uncontrolled transfer, leading to large cracks or folding in the transferred material. Another approach is to develop strategies that allow the direct growth of MoS_2 over the SiN_x aperture, as demonstrated by Waduge et al.[13] where the approach indeed promises scalability and avoids any further contamination with polymer arising from the transfer step. However, growing over apertures is not trivial and typically yields a mix of single and multilayer MoS_2 films. Thus, currently, polymer-based wafer-scale transfer for device fabrication is preferred.[41]

Another challenge is the lack of an efficient nanopore fabrication method that could be employed for wafer-scale fabrication while maintaining pore size reproducibility and distribution. Among all the state-of-art techniques, ion beam irradiation[22] and lithography-based fabrication[59,60] are the most promising. However, they are still facing a number of technical problems which make them not suitable for batch fabrication of single nanopore devices. Ion beam methods are generally used for pore fabrication at a large scale and lack precise pore definition. The lithographic approach on the other hand requires additional steps involving polymer coatings, leading to further, otherwise avoidable, surface contamination. For these reasons, we have used an ECR-based pore drilling method.[61]

2.4. Short DNA Translocations

To demonstrate the applicability of the MoS_2 nanopores, we performed DNA translocations from representative MoS_2 nanopore devices made using the reported growth and transfer method. **Figure 4**a shows the schematic of the experimental setup. The MoS_2 membrane separates the *cis* and *trans* chambers (1 м KCl-Tris EDTA) of the flow cell. We chose two MoS_2 devices from different sites from the wafer and fabricated a single nanopore in each device using our previously reported electrochemical reaction (ECR) method.[61] In this method, a nanopore is induced by applying a voltage across the membrane to electrochemically etch the MoS_2 at defect sites. The I–V measurement of Device A in 1 м KCl are shown in Figure S10 (Supporting Information). The pore size obtained was 3.6 nm which is typically calculated from the open pore conductance using the well-established conductance model for cylindrical pores.[62] However, differences in ion mobilities of K^+ and Cl^- can affect the estimation of the nanopore sizes for sub 5 nm pores in MoS_2.[63] Since in our case, the nanopore sizes are below 5 nm, our nanopore diameter using the estimation proposed by Perez et al.[63] is ≈3.9 nm. We then set out to measure short DNA translocations through this nanopore. No translocation signals occur in the absence of DNA (negative control) in any of these devices. We then added 100 bp dsDNA (a final concentration of 20×10^{-9} м) to the *cis*-compartment (1 м KCl, TE-buffer, pH 7.5) and electrophoretically translocated the DNA molecules through the nanopore. The translocations were performed at 500 mV at room temperature (≈24 °C). We recorded a total number of 1266 events which were fitted using a CUSUM algorithm.[64] A representative 10 s concatenated current-time trace showing 100 bp DNA translocations at 500 mV is shown in Figure 4b. The ion-current baseline fluctuations are associated with charge interactions occurring at the rim of the nanopore[65]

© 2020 WILEY-VCH Verlag GmbH & Co. KGaA, Weinheim

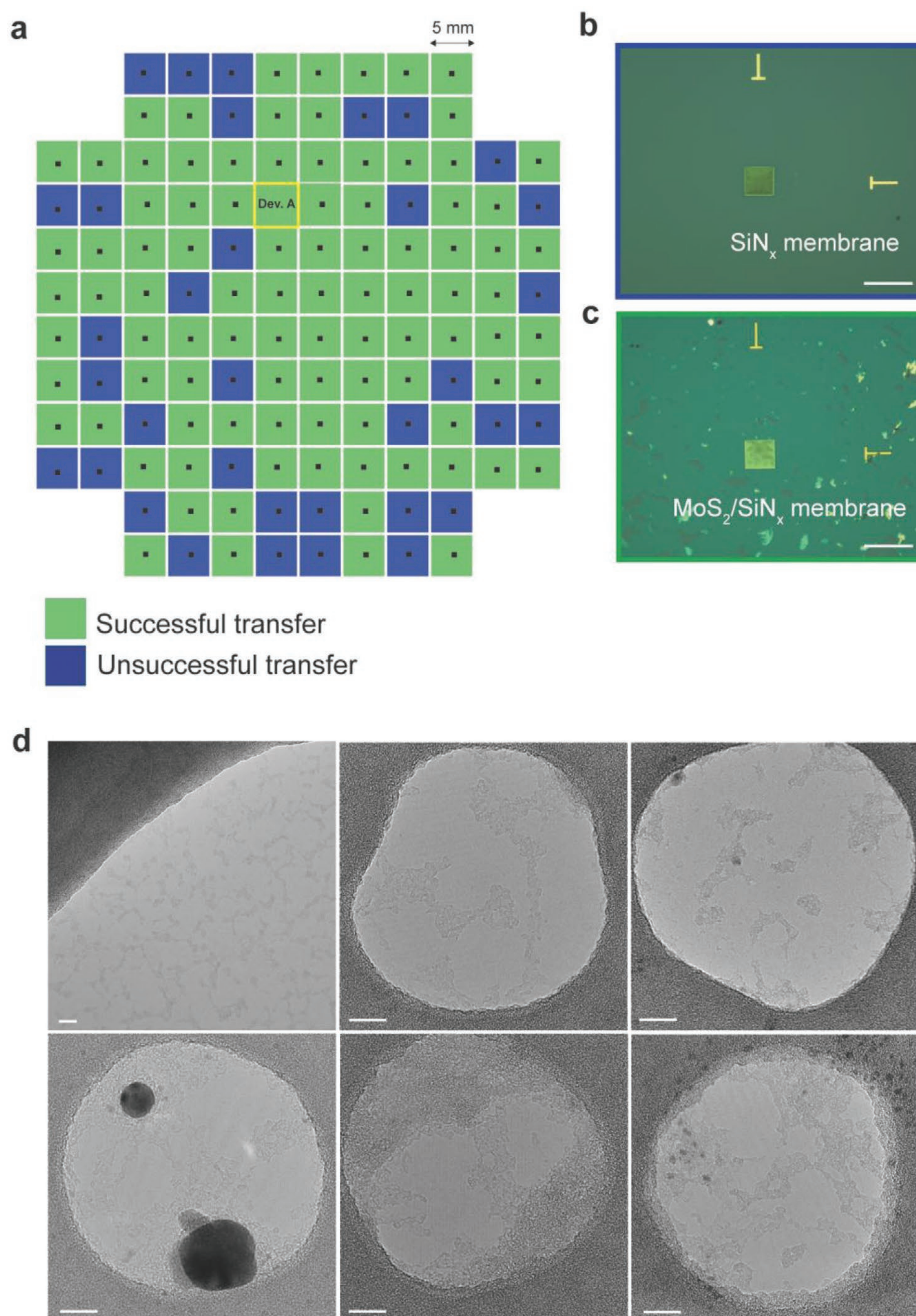

Figure 3. a) Color-map showing the wafer-scale transfer efficiency of MoS_2 over the SiN_x membrane using PDMS. The devices and their transfer is represented as complete (n = 94, green) or unsuccessful transfer (n = 34, blue). b) A representative substrate before transfer and c) after transfer to the SiN_x membrane. All scale bars are 50 µm. d) TEM imaging of suspended MoS_2 after transfer. The devices show MoS_2 regions with few polymer residues after transfer. All scale bars are 10 nm.

as well as the mechanical fluctuations of the thin suspended 2D material.[66] A few representative events from the trace are shown in Figure 4c. Figure 4d shows a scatter plot of all the fitted events obtained from Device A at 500 mV with a MoS_2 nanopore. We observed a relative current blockade of ≈20–25%, which corresponds well to the expected fractional current blockade (≈25%) of dsDNA.[14] Most of the recorded events for 100 bp DNA show an average dwell time less than 200 µs, while some events span over a millisecond. The bandwidth of our system is about 10 kHz, which can lead to distortions of events shorter than ≈50 µs.[67] The dwell time distribution is associated with the limited bandwidth of the measurement, leading to the invisibility of fast translocation events.[68] The longer dwell time for the events seen in Figure 4c,d can arise from interaction

 © 2020 WILEY-VCH Verlag GmbH & Co. KGaA, Weinheim

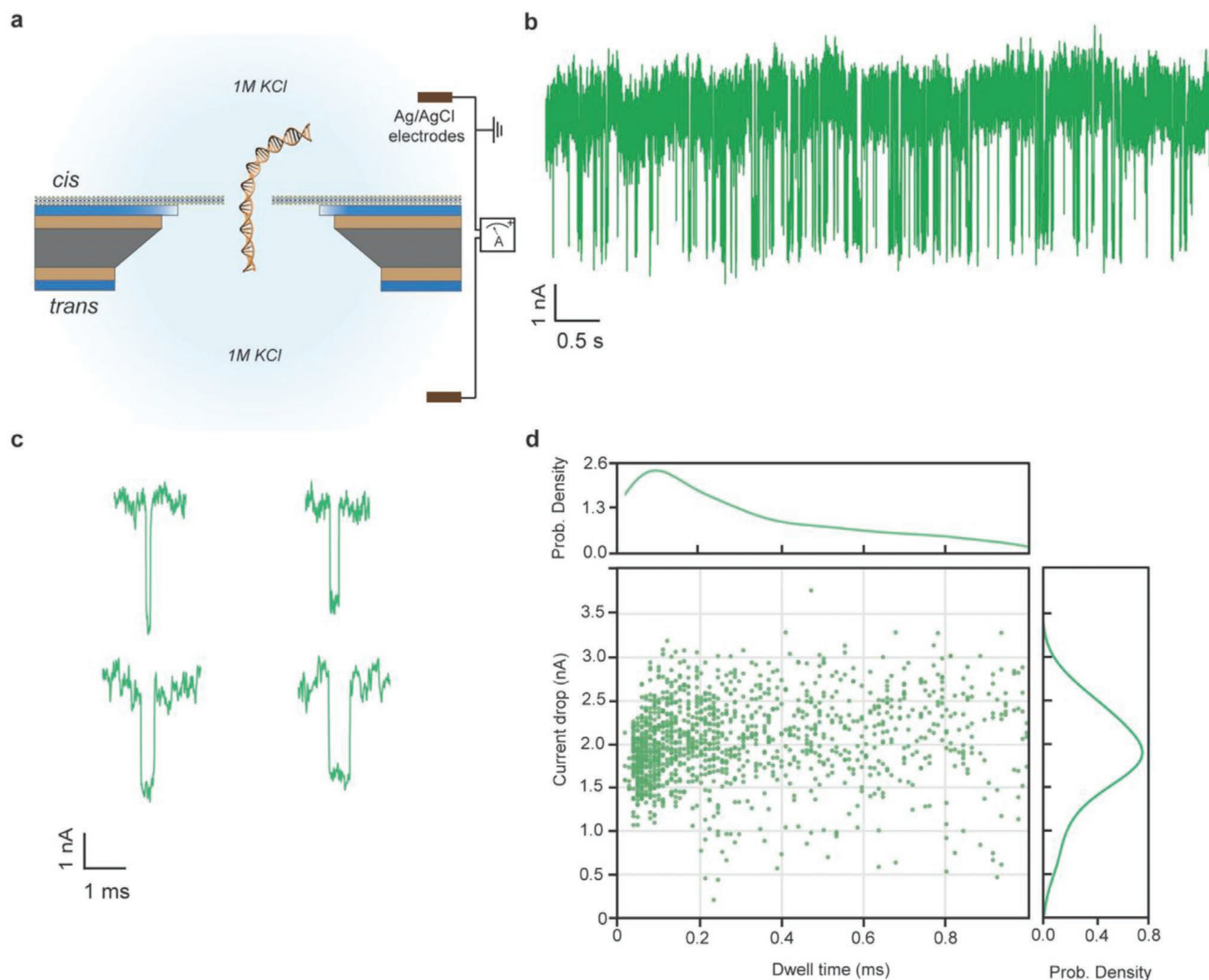

Figure 4. Short double-stranded (ds)DNA translocations through a MoS_2 nanopore (Device A). a) Schematic showing the setup for the translocation experiment (not to scale). b) Concatenated 10 s trace of 100 bp dsDNA recorded in 1 м KCl. The data was recorded at 500 mV, low-pass filtered at 10 kHz, and digitized at 100 kHz. c) Representative events from the trace shown in (b). d) All-point scatter-plot and probability density estimation of the current drop versus dwell time (n = 1266).

of the DNA with MoS_2 around nanopore surface before completely threading through the pore. Both ssDNA and dsDNA are known to interact with MoS_2 surface albeit with different affinities[15,69] which might increase their residence time in the pore thereby increasing their dwell time. The nucleobases of the ssDNA are exposed which is in contrast to dsDNA. These exposed nucleobases interact with the MoS_2 surface via van der Waals (vdW) interactions.[69,70] These nucleobases possess differential affinity toward transition metal dichalcogenides (e.g., MoS_2 and WS_2) and they interact via vdW forces.[71] The vdW interaction for adsorption is facilitated by a large electronegativity difference between Mo-atoms and S-atoms of MoS_2. Molecular dynamic simulations show that the MoS_2 nanopore edge also play an important role in the sticking behavior of both ssDNA and dsDNA.[18] The MoS_2 nanopore with higher Mo-atoms (hydrophilic) termination interacts less to the DNA (hydrophobic) in comparison to S-atom (hydrophilic) termination. In solid-state silicon nitride pores, it has been observed that due to interaction with the nanopore, the fluctuations of the DNA is stabilized.[72] Thus the residence time of the DNA can be influenced by the interaction with the nanopore edges as well as the surface of the material. Furthermore, we show 100 bp translocation at lower voltages in another MoS_2 nanopore Device B from different batch with similar pore diameter (≈4 nm) fabricated using the same ECR method (the details of this experiment are shown in Figure S11, Supporting Information).

3. Conclusion

In conclusion, we demonstrated large-area manufacturing of MoS_2 nanopore devices by wafer-scale growth, fabrication and transfer of MoS_2 films. We show that the fabrication of 128 devices on a single 10.16 cm wafer can be performed with >70% efficiency. With the current technique, it is possible to

© 2020 WILEY-VCH Verlag GmbH & Co. KGaA, Weinheim

further scale-up by using higher density of devices and transfer of large-area 2D materials. The MoS_2 quality and the nanopore devices were clean at the atomic scale as confirmed by TEM and STEM imaging. The single-nanopores were created by the ECR method. Unlike TEM-based nanopore drilling, by electrically isolating each device from each other, this method has the potential for simultaneous creation of nanopores in-situ making it a scalable method of single nanopores production on the same wafer. In the end, we showed the applicability of our devices for biosensing of short 100 bp DNA molecules. In principle, these devices can be used for other exciting applications involving wafer-scale flexible electronics[41,73–75] as well as highly efficient osmotic energy harvesting cells[24] or recently emerged extension of nanopore sequencing–a nanopore field-effect transistors enabling both ionic and transverse current based biomolecule detection.[15,76,77] We believe that further integration and parallelization of nanopore based membrane devices will lead to high-throughput usage[78–81] and in turn will encourage new, emerging, commercial applications of this technology.

4. Experimental Section

Wafer-Scale Growth of MoS_2: Prior to the growth, 7.62 cm c-plane sapphire wafers (MTI) were cleaned with IPA, acetone and DI, annealed in 1000 °C for 6 h to obtain an atomically smooth surface, treated with potassium hydroxide solution (Sigma Aldrich, 99.0%) for 30 min, rinsed with DI water, dried, and finally spin-coated with a growth promoter in aqueous solution of 0.03 M Na_2MoO_4 (Sigma Aldrich, 98.0%) and 0.1 M NaCl (Sigma Aldrich, 99.5%). MoS_2 film synthesis was performed in a 10.16 cm hot-wall tube furnace (MTI OTF-1200X-II). For carrier and process gases ultra high purity Ar (Carbagas, 99.999%), H_2 (Vici DBS NM Plus 100 Hydrogen Generator, purity 99.999%), and O_2 (Carbagas, 99.9%) were used. Molybdenum hexacarbonyl ($Mo(CO)_6$, Sigma Aldrich, 99.9%) and diethyl sulfide ($C_2H_6S_2$, Sigma Aldrich, 98.0%) were used for metalorganic precursor and reaction gas respectively, and were kept in separate bubblers maintained at stable 17 °C and room pressure. Spin-coated sapphire substrates were then loaded vertically in a quartz boat placed inside the reactor tube. This position ensures perpendicular exposure to the gas flow, thus ensuring axial growth uniformity. Furnace was then filled with Ar, ramped up to 120 °C and held under carrier Ar flow of 210 sccm for 30 min to dry the reactor walls of adsorbed water molecules. After this step, the reactor was ramped to 850 °C at a rate of 20 °C min^{-1}. The growth step was initiated by injecting 4 sccm of H_2, 1 sccm of O_2 and precursor gases. With an argon flow of 12 sccm for $Mo(CO)_6$ and 3 sccm for DES through both bubblers, the actual mass flow of $Mo(CO)_6$ and DES at 17 °C and at ambient pressure was 4.40×10^{-4} sccm and 2.50×10^{-1} sccm, respectively. After the growth step, the furnace was cooled down to room temperature naturally. To avoid MoS_2 deterioration, samples were kept in a dry atmosphere between all of the subsequent transfer and characterization steps.

Nanopore Substrate Fabrication: Double-side polished 100 mm (100) undoped Si-wafers (produced by Active Business Company) were covered with 60 nm of SiO_2 and 20 nm low-stress SiN_x from both sides (done by supplier). Photolithography and dry etching were done to open apertures in the back side SiN_x layer for the subsequent wet etching process required for SiN_x membrane formation on the front-side. Front-side e-beam lithography and dry etching were performed to form 80 nm-diameter apertures in SiN_x membranes with the following parameters: 100 kV e-beam voltage, polymethyl methacrylate (PMMA, molecular weight 495 K, 4% in anisole) as e-beam resist (EBR) and CHF_3/O_2 gas mixture for dry etching. As a final step acid piranha cleaning was done to achieve clean surface of the target nanopore substrate prepared for the further MoS_2 transfer.

MoS2 Transfer: PDMS-assisted transfer of 7.61 cm MoS_2 films were used from the sapphire wafer to the SiN_x wafer assisted by water.[38] The PDMS base reagent and curing agent were mixed in a 10:1 ratio and cured on a 10.16 cm Si-wafer for 4 h at 80 °C. The PDMS was then cut, peeled off, and attached to a custom-made translation stage (MTS25A-Z8, Thorlabs) motorized by a DC Servo. For the complete lift-off process, one edge of the PDMS is attached to the translation stage while the PDMS is carefully placed on MoS_2/sapphire substrate. During this step a special care should be taken to avoid any air gaps or dust on the polymer/substrate interface. The PDMS/MoS_2/sapphire is then placed in a clean container and filled with pre-filtered (20 nm) DI-water. To preserve an entire 7.62 cm area of MoS_2 and ensure complete delamination a slow, controlled lift-off speed of 5–10 µm s^{-1} was used. As a result, the PDMS slowly lifts off MoS_2 from the sapphire as the water penetrates below the MoS_2, enabling the attachment of MoS_2 to the PDMS surface. Further, PDMS/MoS_2 were manually placed onto the SiN_x wafer in an all dry-transfer stamping technique. The PDMS was then peeled off with the translation motor to complete the transfer of MoS_2 on SiN_x wafer. After the transfer process was complete, the SiN_x wafer was annealed at 250 °C (8 h) in argon and hydrogen (100 and 10 sccm, respectively) environment.

Characterization: Atomic force microscopy was performed on the Asylum Research Cypher AFM system with tapping mode. Raman and PL spectroscopy were done with a Renishaw inVia Confocal Raman Microscope with a 532 nm laser beam at a low power (<0.3 mW) to avoid defect nucleation and substrate damage. A diffraction grating of 3000 mm^{-1} was used for good spatial resolution. Transmission electron microscopy was performed on a FEI TEM Talos at 80 kV acceleration voltage in high-resolution TEM (HRTEM) mode. Prior to imaging, moderate substrate heating was performed in air (160 °C for 30 min) to minimize contamination and unwanted electron beam induced deposition of hydrocarbons. Scanning transmission electron microscopy imaging experiments were conducted using an aberration-corrected (with double Cs corrector) FEI Titan Themis TEM 60–300 kV, equipped with Schottky X-FEG electron source and a monochromator to reduce the effect of chromatic aberrations. To avoid sample damage, a low acceleration voltage (80 kV) was used for all the experiments, which is below the electron-beam induced knock-on damage of MoS_2. The typical electron probe current was 18 pA. Images were acquired with a Gatan high angle annular dark field (HAADF) detector with angular range (49.5–198 mrad) using 185 mm camera length. To highlight the relevant detail, the image was processed using the "double-Gaussian filtering" method.[50]

DNA Translocations: The MoS_2 devices were assembled in a customized PMMA flow cell. The flow cell design and assembling steps are explained in detail elsewhere.[14] Then the flow cell was filled with 1 M KCl, 10×10^{-3} M Tris and 100×10^{-3} M EDTA buffered at pH = 7.5 (20 nm filtered, degassed) and the nanopores in MoS_2 were made by the ECR technique. Once the desired pore size was obtained, the translocation measurements were performed. NoLimits 100 bp DNA Fragment (Thermo Fisher Scientific, USA) was briefly preheated at 65–70 °C followed by cooling down to room temperature prior to the experiment to ensure proper dispersion of the DNA molecules in the buffer and helps to avoid clogging of the nanopore.[82,83] The 100 bp DNA was then added to the *cis*-compartment of the flow cell and a voltage was applied to electrophoretically translocate DNA through the nanopore. The data acquisition was performed using an Axopatch 200B (Axon Instruments, USA) low-pass filtered at 10 kHz and recorded at a 100 kHz sampling rate. The data analysis, event detection and plotting was done using the Python-based OpenNanopore toolkit (https://www.epfl.ch/labs/lben/opennanopore-python).

Supporting Information

Supporting Information is available from the Wiley Online Library or from the author.

© 2020 WILEY-VCH Verlag GmbH & Co. KGaA, Weinheim

Acknowledgements

M.T. and M.M. contributed equally to this work. This work was financially supported by a Swiss National Science Foundation (SNSF) Consolidator grant (BIONIC BSCGI0_157802), and by a CCMX project ("Large Area Growth of 2D Materials for device integration"). Device fabrication was partially carried out at the Center for Micro/Nanotechnology (CMi) at EPFL. The authors thank the Centre Interdisciplinaire de Microscopie Electronique (CIME) at EPFL for access to electron microscopes. A.C. acknowledges the funding through Eurotech Postdoc Programme (European Commission Horizon 2020. Grant Agreement number 754462).

Conflict of Interest

The authors declare no conflict of interest.

Keywords

2D materials, biosensing, growth, molybdenum disulfide, nanopores, transfer, wafer-scale

Received: February 3, 2020
Revised: March 15, 2020
Published online: May 11, 2020

[1] F. Haque, J. Li, H.-C. Wu, X. J. Liang, P. Guo, *Nano Today* **2013**, *8*, 56.
[2] B. M. Venkatesan, R. Bashir, *Nat. Nanotechnol.* **2011**, *6*, 615.
[3] C. Dekker, *Nat. Nanotechnol.* **2007**, *2*, 209.
[4] S. Hernández-Ainsa, U. F. Keyser, *Nanomedicine* **2013**, *8*, 1551.
[5] T. Z. Butler, M. Pavlenok, I. M. Derrington, M. Niederweis, J. H. Gundlach, *Proc. Natl. Acad. Sci. USA* **2008**, *105*, 20647.
[6] H. Lu, F. Giordano, Z. Ning, Z. Genomics, *Proteomics Bioinf.* **2016**, *14*, 265.
[7] C. A. Merchant, K. Healy, M. Wanunu, V. Ray, N. Peterman, J. Bartel, M. D. Fischbein, K. Venta, Z. Luo, A. T. C. Johnson, M. Drndić, *Nano Lett.* **2010**, *10*, 2915.
[8] G. F. Schneider, S. W. Kowalczyk, V. E. Calado, G. Pandraud, H. W. Zandbergen, L. M. K. Vandersypen, C. Dekker, *Nano Lett.* **2010**, *10*, 3163.
[9] K. Liu, L. Martina, S. Aditya, S. Caneva, H. Qiu, D. Deiana, V. Tileli, D. T. L. Alexander, S. Hofmann, D. Dumcenco, A. Kis, J -P. Leburton, A. Radenovic, *Nano Lett.* **2017**, *17*, 36.
[10] G. Danda, P. M. Das, Y. C. Chou, J. T. Mlack, W. M. Parkin, C. H. Naylor, K. Fujisawa, T. Zhang, L. B. Fulton, M. Terrones, A. T. C. Johnson, M. Drndić, *ACS Nano* **2017**, *11*, 1937.
[11] K. Liu, J. Feng, A. Kis, A. Radenovic, *ACS Nano* **2014**, *8*, 2504.
[12] J. Feng, K. Ke Liu, R. D. Bulushev, S. Khlybov, D. Dumcenco, A. Kis, A. Radenovic, *Nat. Nanotechnol.* **2015**, *10*, 1070.
[13] P. Waduge, B. Ismail, L. Joseph, Y. H. Robert, G. Kenneth, A. C. Graham, D. C. Bell, N. Vamivakas, S. Kar, M. Wanunu, *ACS Nano* **2015**, *9*, 7352.
[14] M. Graf, L. Martina, M. Thakur, V. Georgiou, J. Topolancik, B. R. Ilic, K. Liu, J. Feng, Y. Astier, A. Radenovic, *Nat. Protoc.* **2019**, *14*, 1130.
[15] M. Graf, M. Lihter, D. Altus, S. Marion, A. Radenovic, *Nano Lett.* **2019**, *19*, 9075.
[16] K. Liu, C. Pan, A. Kuhn, A. P. Nievergelt, G. E. Fantner, O. Milenkovic, A. Radenovic, *Nat. Commun.* **2019**, *10*, 1.
[17] B. Radisavljevic, A. Radenovic, J. Brivio, V. Giacometti, A. Kis, *Nat. Nanotechnol.* **2013**, *6*, 147.
[18] A. B. Farimani, M. Kyoungmin, N. R. Aluru, *ACS Nano* **2014**, *8*, 7914.
[19] J. P. Thiruraman, F. K. Fujisawa, G. Danda, P. M. Das, T. Zhang, A. Bolotsky, P. L. Nestor, P. Senet, M. Terrones, M. Drndić, *Nano Lett.* **2018**, *18*, 1651.
[20] G. Danda, M. Drndić, *Curr. Opin. Biotechnol.* **2019**, *55*, 124.
[21] R. Kozubek, M. Tripathi, M. Ghorbani-Asl, S. Kretschmer, L. Madaub, E. Pollmann, M. O'Brien, N. McEvoy, U. Ludacka, T. Susi, G. Duesberg, R. Wilhelm, A. Krasheninnikov, J. Kotakoski, M. Schleberger, *J. Phys. Chem. Lett.* **2019**, *10*, 904.
[22] J. P. Thiruraman, P. M. Das, M. Drndić, *Adv. Funct. Mater.* **2019**, *29*, 1904668.
[23] J. A. Ke, S. Garaj, S. Gradečak, *ACS Appl. Mater. Interfaces* **2019**, *11*, 26228.
[24] M. Macha, S. Marion, V. V. R. Nandigana, A. Radenovic, *Nat. Rev. Mater.* **2019**, *4*, 588.
[25] J. Feng, G. Michael, L. Ke, D. Ovchinnikov, D. Dumcenco, M. Heiranian, V. Nandigana, N. R. Aluru, A. Kis, A. Radenovic, *Nature* **2016**, *536*, 197.
[26] M. Graf, M. Lihter, D. Unuchek, A. Sarathy, J.-P. Leburton, A. Kis, A. Radenovic, *Joule* **2019**, *3*, 1549.
[27] A. Castellanos-Gomez, M. Buscema, R. Molenaar, V. Singh, L. Janssen, H. S. J. Van Der Zant, G. A. Steele, *2D Mater.* **2014**, *1*, 011002.
[28] R. Frisenda, E. Navarro-Moratalla, P. Gant, D. Pérez De Lara, P. Jarillo-Herrero, R. V. Gorbachev, A. Castellanos-Gomez, *Chem. Soc. Rev.* **2018**, *47*, 53.
[29] K. Kang, S. Xie, L. Huang, Y. Han, P. Y. Huang, K. F. Mak, C.-J. Kim, D. Muller, J. Park, *Nature* **2015**, *520*, 656.
[30] S. Boandoh, S. H. Choi, J. H. Park, S. Y. Park, S. Bang, M. S. Jeong, J. S. Lee, H. J. Kim, W. Yang, W. C. Jae Young, K. Soo Min, K. Ki Kang, *Small* **2017**, *13*, 1701306.
[31] H. Cun, M. Macha, H. Kim, K. Liu, Y. Zhao, T. LaGrange, A. Kis, A. Radenovic, *Nano Res.* **2019**, *12*, 2646.
[32] J. Zhou, J. Lin, X. Huang, Y. Zhou, Y. Chen, J. Xia, H. Wang, Y. Xie, H. Yu, J. Lei, D. Wu, F. Fucai, Q. Qundong, Q. Zeng, C.-H. Hsu, C. Yang, L. Lu, T. Yu, Z. Shen, H. Lin, B. I. Yakobson, Q. Liu, K. Suenaga, G. Liu, Z. Liu, *Nature* **2018**, *556*, 355.
[33] D. Dumcenco, O. Dmitry, M. Kolyo, P. Lazić, M. Gibertini, N. Marzari, O. Lopez Sanchez, O. L. Sanchez, Y.-C. Kung, D. Krasnozhon, M. W. Chen, S. Bertolazzi, P. Gillet, A. Fontcuberta, I. Morral, A. Radenovic, A. Kis, *ACS Nano* **2015**, *9*, 4611.
[34] H. Kim, H. Ovchinnikov, D. Deiana, D. Unuchek, A. Kis, *Nano Lett.* **2017**, *17*, 5056.
[35] H. Li, J. Wu, X. Huang, Z. Yin, J. Liu, H. Zhang, *ACS Nano* **2014**, *8*, 6563.
[36] A. Gurarslan, Y. Yu, L. Su, Y. Yu, F. Suarez, S. Yao, Y. Zhu, M. Ozturk, Y. Zhang, L. Cao, *ACS Nano* **2014**, *8*, 11522.
[37] Z. Lu, L. Sun, G. Xu, J. Zheng, Q. Zhang, J. Wang, L. Jiao, *ACS Nano* **2016**, *10*, 5237.
[38] H. Yu, M. Liao, W. Zhao, G. Liu, X. J. Zhou, Z. Wei, X. Xu, K. Liu, Z. Hu, K. Deng, S. Zhou, J. A. Shi, L. Gu, C. Shen, T. Zhang, L. Du, L. Xie, J. Zhu, W. Chen, R. Yang, D. Shi, G. Zhang, *ACS Nano* **2017**, *11*, 12001.
[39] M. Meitl, Z. Zhu, V. Kumar, K. Lee, X. Feng, Y. Huang, I. Adesida, R. G. Nuzzo, J. A. Rogers, *Nat. Mater.* **2006**, *5*, 33.
[40] M. Xuezhi, Q. Liu, D. Xu, Y. Zhu, S. Kim, Y. Cui, L. Zhong, M. Liu, *Nano Lett.* **2017**, *17*, 6961.
[41] S. Shinde, T. Das, A. Hoang, B. Sharma, X. Chen, J. H. Ahn, *Adv. Funct. Mater.* **2018**, *28*, 1.
[42] Q. H. Thi, H. Kim, J. Zhao, J. T. H. Ly, *npj 2D Mater. Appl.* **2018**, *2*, 34.
[43] K. C Kwon, C. Seokhoon, K. Hong, C. W. Moon, Y. S. Shim, D. H. Kim, T. Kim, W. Sohn, J. M. Jeon, C. H. Lee, K. T. Nam, S. Han, S. Y. Kim, H. W. Jang, *Energy Environ. Sci.* **2016**, *9*, 2240.
[44] A. Jain, P. Bharadwaj, S. Heeg, M. Parzefall, T. Taniguchi, K. Watanabe, L. Novotny, *Nanotechnology* **2018**, *29*, 265203.

© 2020 WILEY-VCH Verlag GmbH & Co. KGaA, Weinheim

[45] J. T. Mlack, P. M. Das, G. Danda, Y.-C. Chou, C. H. Naylor, Z. Lin, N. P. López, T. Zhang, M. Terrones, A. Johnson, M. Drndić, *Sci. Rep.* **2017**, *7*, 43037.
[46] K. Zhang, B. M. Bersch, F. Zhang, N. C. Briggs, S. Subramanian, K. Xu, M. Chubarov, K. Wang, J. O. Lerach, J. M. Redwing, S. K. Fullerton-Shirley, M. Terrones, J. Robinson, *ACS Appl. Mater. Interfaces* **2018**, *10*, 40831.
[47] J. U. Lee, K. Kim, H. Cheong, *2D Mater.* **2017**, *2*, 44003.
[48] B. Chakraborty, A. Bera, D. V. S. Muthu, S. Bhowmick, U. V. Waghmare, A. K. Sood, *Phys. Rev. B* **2012**, *85*, 161403.
[49] D. Ma, J. Shi, Q. Ji, K. Chen, J. Yin, Y. Lin, Y. Zhang, M. Liu, Q. Feng, X. Song, X. Guo, J. Zhang, Y. Zhang, Z. Liu, *Nano Res.* **2015**, *8*, 3662.
[50] O. L. Krivanek, M. F. Chisholm, V. Nicolosi, T. J. Pennycook, G. J. Corbin, N. Dellby, M. F. Murfitt, C. Own, Z. Szilagyi, M. Oxley, S. Pantelides, S. Pennycook, *Nature* **2010**, *464*, 571.
[51] P. Y. Huang, C. S. Ruiz-Vargas,, A. M. van der Zande, W. S. Whitney, M. P. Levendorf, J. W. Kevek, S. Garg, J. S. Alden, C. J. Hustedt, Y. Zhu, J. Park, P. L. McEuen, D. A. Muller, *Nature* **2011**, *469*, 389.
[52] W. Zhou, X. Zou, S. Najmaei, Z. Liu, Y. Shi, J. Kong, J. Lou, A. Pulickel, B. I. Yakobson, J.-C. Idrobo, *Nano Lett.* **2013**, *13*, 2615.
[53] H.-P. Komsa, J. Kotakoski, S. Kurasch, O. Lehtinen, U. Kaiser, A. V. Krasheninnikov, *Phys. Rev. Lett.* **2012**, *109*, 35503.
[54] J. Hong, H. Zhixin, M. Probert, K. Li, D. Lv, X. Yang, L. Gu, N. Mao, Q. Feng, L. Xie, J. Zhang, D. Wu, Z. Zhang, C. Jin, W. Ji, X. Zhang, J. Yuan, Z. Zhang, *Nat. Commun.* **2015**, *6*, 1.
[55] C. Holroyd, A. B. Horn, C. Casiraghi, S. P. K. Koehler, *Carbon* **2017**, *117*, 473.
[56] A. Kozbial, X. Gong, H. Liu, L. Li, *Langmuir* **2015**, *31*, 8429.
[57] M. Khalkhali, H. Zhang, Q. Liu, *J. Phys. Chem. C* **2018**, *122*, 6737.
[58] J. Yang, M. Choi, Y. Sheng, J. Jung, K. Bustillo, T. Chen, S - W. Lee, P. Ercius, J. H. Kim, J. H. Warner, E. M. Chan, H. Zheng, *Nano Lett.* **2019**, *19*, 1788.
[59] D. V. Verschueren, W. Yang, C. Dekker, *Nanotechnology* **2018**, *29*, 145302.
[60] R. Dela Torre, J. Larkin, A. Singer, A. Meller, *Nanotechnology* **2012**, *23*, 385308.
[61] J. Feng, K. Liu, M. Graf, M. Lihter, R. D. Bulushev, D. Dumcenco, D. T. L. Alexander, D. Krasnozhon, T. Vuletic, A. Kis, A. Radenovic, *Nano Lett.* **2015**, *15*, 3431.
[62] S. W. Kowalczyk, Y. Rabin, A. Y. Grosberg, C. Dekker, *Nanotechnology* **2011**, *22*, 315101.
[63] M. D. B. Pérez, A. Nicolaï, P. Delarue, V. Meunier, M. Drndić, P. Senet, *Appl. Phys. Lett.* **2019**, *114*, 23107.
[64] C. Raillon, P. Granjon, M. Graf, L. J. Steinbock, A. Radenovic, *Nanoscale* **2012**, *4*, 4916.
[65] A. Fragasso, S. Schmid, C. Dekker, *ACS Nano* **2020**, *14*, 1338.
[66] S. J. Heerema, G. F. Schneider, M. Rozemuller, L. Vicarelli, H. W. Zandbergen, C. Dekker, *Nanotechnology* **2015**, *26*, 074001.
[67] Z. Gu, Y. L. Ying, C. Cao, Y. T. Long, P. He, *Anal. Chem.* **2015**, *87*, 907.
[68] S. Carson, J. Wilson, A. Aksimentiev, M. Wanunu, *Biophys. J.* **2014**, *107*, 2381.
[69] C. Zhu, Z. Zeng, H. Li, F. Li, C. Fan, H. Zhang, *J. Am. Chem. Soc.* **2013**, *135*, 5998.
[70] C. Lu, Y. Liu, Y. Ying, J. Liu, *Langmuir* **2017**, *33*, 630.
[71] H. Vovusha, B. Sanyal, *RSC Adv.* **2015**, *5*, 67427.
[72] X. Shi, L. Qiao, R. Gao, W. Si, S. C. Liu, A. Aksimentiev, Y. T. Long, *J. Phys. Chem. Lett.* **2018**, *9*, 4686.
[73] W. Lee, Y. Liu, Y. Lee, B. Sharma, S. Shinde, S. Kim, K. Nan, Z. Yan, M. Han, Y. Huang, Y. Zhang, J.-H. Ahn, J. A. Rogers, *Nat. Commun.* **2018**, *9*, 1417.
[74] X. Chen, Y. Park, M. Kang, S - K. Kang, J. Koo, S. Shinde, J. Shin, S. Jeon, G. Park, Y. Yan, M. MacEwan, W. Ray, K. Lee, J. A. Rogers, J - H. Ahn, *Nat. Commun.* **2018**, *9*, 1690.
[75] E. Singh, P. Singh, K. S. Kim, G. Y. Yeom, H. S. Nalwa, *ACS Appl. Mater. Interfaces* **2019**, *11*, 11061.
[76] A. Fanget, F. Traversi, S. Khlybov, P. Granjon, A. Magrez, L. Forró, A. Radenovic, *Nano Lett.* **2014**, *14*, 44.
[77] M. Puster, J. A. Rodríguez-Manzo, A. Balan, M. Drndić, *ACS Nano* **2013**, *7*, 11283.
[78] T. Jain, B. C. Rasera, R. J. S. Guerrero, J - M. Jim, R. Karnik, *J. Phys.: Condens. Matter* **2017**, *29*, 484001.
[79] J. K. Rosenstein, M. Wanunu, C. A. Merchant, M. Drndić, K. L. Shepard, *Nat. Methods* **2012**, *9*, 487.
[80] M. Zhang, C. Ngampeerapong, D. Redin, A. Ahmadian, I. Sychugov, J. Linnros, *ACS Nano* **2018**, *12*, 4574.
[81] M. Zhang, T. Schmidt, A. Jemt, P. Sahlén, I. Sychugov, J. Lundeberg, J. Linnros, *Nanotechnology* **2015**, *26*, 314002.
[82] C. Plesa, D. Verschueren, S. Pud, J. van der Torre, J. W. Ruitenberg, M. J. Witteveen, M. P. Jonsson, A. Y. Grosberg, Y. Rabin, C. Dekker, *Nat. Nanotechnol.* **2016**, *11*, 1093.
[83] Z. Zhou, Y. Hu, H. Wang, Z. Xu, W. Wang, X. Bai, X. Shan, X. Lu, *Sci. Rep.* **2013**, *3*, 3287.

© 2020 WILEY-VCH Verlag GmbH & Co. KGaA, Weinheim